

A variable partially-polarizing beam splitter

Jefferson Flórez,^{1, a)} Nathan J. Carlson,¹ Codey H. Nackle,¹ Lambert Giner,¹ and Jeff S. Lundeen¹

Department of Physics and Centre for Research in Photonics, University of Ottawa, 25 Templeton Street, Ottawa, Ontario K1N 6N5, Canada

(Dated: 13 March 2022)

We present designs for variably polarizing beam splitters. These are beam splitters allowing the complete and independent control of the horizontal and vertical polarization splitting ratios. They have quantum optics and quantum information applications, such as quantum logic gates for quantum computing and non-local measurements for quantum state estimation. At the heart of each design is an interferometer. We experimentally demonstrate one particular implementation, a displaced Sagnac interferometer configuration, that provides an inherent instability to air currents and vibrations. Furthermore, this design does not require any custom-made optics but only common components which can be easily found in an optics laboratory.

I. INTRODUCTION

Typical polarizing beam splitters are intended to spatially separate the horizontal (H) and vertical (V) polarization components of an input beam. However, there are several applications in which a particular set of transmission and reflection coefficients for each polarization are required, like in quantum logic gates^{1–3}, quantum state estimation techniques^{4,5}, and wave-particle duality studies⁶. A device that provides such coefficients is called a partially-polarizing, or polarization-dependent, beam splitter (PPBS). To illustrate its properties, consider a PPBS illuminated by a diagonally polarized beam, as shown in Fig. 1. Depending on the values of the transmission (T) and reflection (R) coefficients for H and V , one can have any chosen splitting ratio (i.e., $T:R$) between the two PPBS output ports independently for the horizontally and vertically polarized light.

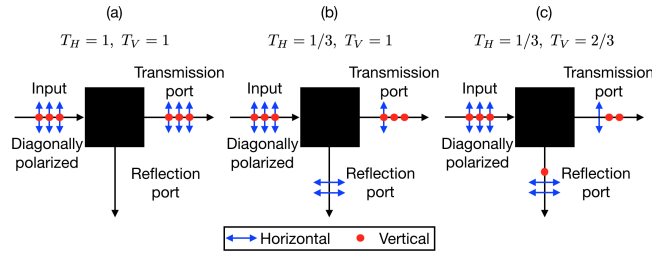


FIG. 1. Schematic representation of a partially-polarizing beam splitter. If $T_H = 1 = T_V$ as in panel (a), one will have both the horizontally and vertically polarized light being transmitted by the PPBS, whereas there will be no light coming out at the reflection port. If $T_H = 1/3$ and $T_V = 1$ as in panel (b), one will have one third of the incoming horizontally polarized light being transmitted and the rest reflected, whereas all the vertically polarized light is transmitted by the PPBS. Finally, if $T_H = 1/3$ and $T_V = 2/3$ as in panel (c), one third and two thirds of the horizontally and vertically polarized light are transmitted, respectively, and the rest is reflected.

A PPBS can be built using multilayered dielectric coatings designed for specific T and R coefficients for each polarization. The drawback of this custom fabricated beam splitter is that such coefficients cannot be tuned for different purposes, including the correction of fabrication caused deviations from the target values of T and R . These can lead to a reduced performance in some applications⁶. Moreover, these devices are not available off-the-shelf and are, thus, expensive. In this paper, a *variable* partially-polarizing beam splitter (VPPBS) is introduced featuring a complete and independent control of the horizontal and vertical T and R coefficients. Furthermore, it is based on bulk optical components that are usually available in any optics laboratory.

The working principle of the VPPBS presented here is the interference of two beams in a simple interferometer like a Mach-Zehnder. Consider light entering only one input of the first beam splitter in that interferometer, as shown in Fig. 2. Light interferes constructively or destructively at the last beam splitter depending on the phase between the two optical paths. It follows that the interferometer input light can be made to exit the last beam splitter entirely via Output 1 or, alternately, entirely via Output 2, or some combination of the two output ports. By tuning the interferometer phase one can set any desired splitting ratio between these two output ports. Considered in its entirety, the Mach-Zehnder is a beamsplitter, with Output 1 and 2 arbitrarily defined as the effective transmission and reflection beamsplitter ports. And so, one can vary the beam splitter T and R coefficients by varying the phase. Now consider both H and V entering the interferometer input. By tuning the phase for each of these polarizations independently the splitting ratios for H and V can be set independently. With this independent phase control, the Mach-Zehnder is a VPPBS.

II. THEORY

In this section a theoretical description of the VPPBS mechanism outlined above is presented. (For completeness, in Appendix A, a theoretical description of a nom-

^{a)}Electronic mail: jflor020@uottawa.ca

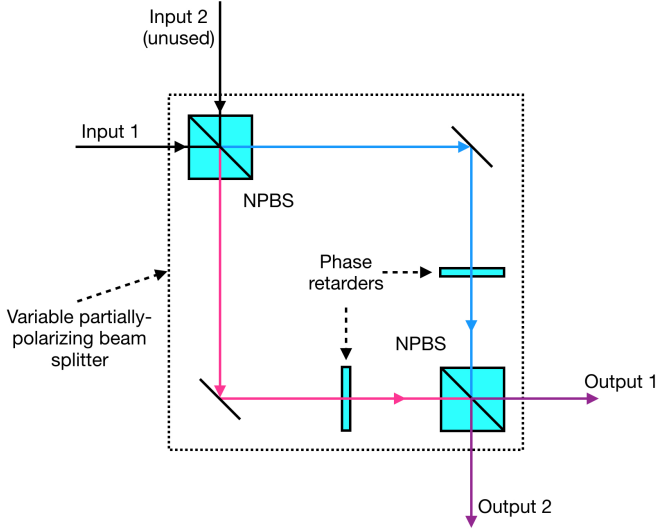


FIG. 2. The basis of the variable partially-polarizing beam splitter (VPPBS) presented here is two independent interference processes occurring in a Mach-Zehnder interferometer, one for the horizontal and the other for the vertical polarization. The phase retarders introduce polarization-dependent phases between the two optical paths. Outputs 1 and 2 play the role of the transmission and reflection VPPBS ports, respectively. NPBS is a non-polarizing 50:50 beam splitter. That is, a beam-splitter with $T = R = 1/2$ for both polarizations.

inally distinct, but actually closely related, configuration is presented based on polarizing beam splitters in the place of non-polarizing beam splitters.) Consider an incoming light beam entering at Input 1 of the Mach-Zehnder interferometer in Fig. 2. In the H/V basis, such a light beam is characterized by an electric field $\mathbf{E}_{\text{in}}(t)$ of the form

$$\mathbf{E}_{\text{in}}(t) = \begin{bmatrix} E_{\text{in}}^H(t) \\ E_{\text{in}}^V(t) \end{bmatrix}, \quad (1)$$

where $E_{\text{in}}^H(t)$ and $E_{\text{in}}^V(t)$ are the H and V polarization components, respectively. After the first 50:50 non-polarizing beam splitter (NPBS) in Fig. 2, the electric fields describing the upper and lower paths just before the phase retarders differ by a phase of $\pi/2$ due to the different number of reflections. This is,

$$\mathbf{E}_{\text{upper}}(t) = \frac{1}{\sqrt{2}}\mathbf{E}_{\text{in}}(t), \quad \mathbf{E}_{\text{lower}}(t) = \frac{e^{i\pi/2}}{\sqrt{2}}\mathbf{E}_{\text{in}}(t). \quad (2)$$

Now, the two phase retarders in the interferometer arms introduce independent phases ϕ_H and ϕ_V to the H and V polarization, respectively. These phase retarders can be, for example, two liquid crystal cells with crystal axes orthogonally oriented to one another, i.e., along either the H or V directions. The electric fields just after the phase retarders and before the second NPBS in Fig.

2 read

$$\tilde{\mathbf{E}}_{\text{upper}}(t) = \frac{1}{\sqrt{2}} \begin{bmatrix} E_{\text{in}}^H(t) \\ e^{i\phi_V} E_{\text{in}}^V(t) \end{bmatrix}, \quad (3)$$

$$\tilde{\mathbf{E}}_{\text{lower}}(t) = \frac{e^{i\pi/2}}{\sqrt{2}} \begin{bmatrix} e^{i\phi_H} E_{\text{in}}^H(t) \\ E_{\text{in}}^V(t) \end{bmatrix}, \quad (4)$$

where it has been assumed without loss of generality that the phase retarder in the upper path introduces the phase ϕ_V , while the one in the lower path introduces ϕ_H . After the second NPBS, i.e. at the outputs of the Mach-Zehnder interferometer, the electric fields become

$$\mathbf{E}_{\text{out},1}(t) = \begin{bmatrix} e^{i\phi_H/2} E_{\text{in}}^H(t) \cos\left(\frac{\phi_H}{2}\right) \\ e^{i\phi_V/2} E_{\text{in}}^V(t) \cos\left(\frac{\phi_V}{2}\right) \end{bmatrix}, \quad (5)$$

$$\mathbf{E}_{\text{out},2}(t) = \begin{bmatrix} -ie^{i\phi_H/2} E_{\text{in}}^H(t) \sin\left(\frac{\phi_H}{2}\right) \\ ie^{i\phi_V/2} E_{\text{in}}^V(t) \sin\left(\frac{\phi_V}{2}\right) \end{bmatrix}. \quad (6)$$

The T coefficient for the horizontal polarization is defined as the ratio between the horizontal light intensity in Output 1 and the intensity of that polarization in the input beam. Similarly, T_V corresponds to the ratio between the vertical light intensity in Output 1 and the initial intensity of such polarization. In terms of Eqs. (5) and (6), this is

$$T_\epsilon \equiv \frac{|E_{\text{out},1}^\epsilon(t)|^2}{|E_{\text{in}}^\epsilon(t)|^2} = \frac{1 + \cos \phi_\epsilon}{2}, \quad (7)$$

where $\epsilon = H, V$. The fields $E_{\text{out},1}^H$ and $E_{\text{out},1}^V$ are, respectively, the H and V components of $\mathbf{E}_{\text{out},1}$. The reflection coefficients for the horizontal and vertical polarizations are given by $R_H = 1 - T_H$ and $R_V = 1 - T_V$, respectively. Thus, by tuning ϕ_H and ϕ_V any possible value of reflection and transmission coefficients can be chosen. This constitutes a VPPBS.

The challenge in this design is how to vary ϕ_H and ϕ_V . As mentioned earlier, one possibility for the phase retarders are orthogonally oriented two liquid crystals. Here, the relative phases ϕ_H and ϕ_V are independently tuned by means of the AC voltage applied to each liquid crystal. Another possibility, which is the one implemented here, is to vary the tilt of a uniaxial birefringent crystal (i.e., one with parallel input and output faces) in one of the interferometer arms. Both the refractive index and optical path length will vary differently for the two polarizations as the element is tilted. In turn, the

introduced phases ϕ_b^H and ϕ_b^V for the the H and V polarizations, respectively, will be differently tuned by the tilt. This will set the phase difference $\Delta\phi = \phi_H - \phi_V$. To achieve full independent control of each phase, tilting a second non-birefringent plate (e.g., glass) can be used to introduce an identical phase ϕ_g offset to the two polarizations, so that

$$\phi_H = \phi_b^H - \phi_g, \quad (8)$$

$$\phi_V = \phi_b^V - \phi_g. \quad (9)$$

In summary, with the two tilts as control parameters, it is possible to independently set the two system degrees of freedom, ϕ_H and ϕ_V .

The relative phase ϕ introduced between the two optical paths in a Mach-Zehnder interferometer by a plate of thickness d and refractive index n is $\phi = 2\pi d(n - n_a)/\lambda$, where n_a is the refractive index of air and λ is the wavelength of light. This expression describes the case when the plate is placed in one arm of the interferometer so that it is normal the beam. In Appendix B, it is shown that if the plate is tilted by θ_p from normal, the relative phase is given by

$$\phi_p^\epsilon = \frac{2\pi d_p}{\lambda} \left[\frac{n_p^\epsilon}{\cos \theta_p^\epsilon} - n_a (\cos \theta_p + \sin \theta_p \tan \theta_p^\epsilon) \right], \quad (10)$$

where $p = b$ or g for the birefringent and glass plates, respectively, and θ_p^ϵ is the angle of light inside the optical medium after refraction. In the case, $p = g$ the ϵ label is not used throughout the paper, whereas for $p = b$, $\epsilon = H, V$. In particular, there are two refractive indices n_b^H and n_b^V for the birefringent medium. The angle θ_p^ϵ is given by Snell's law,

$$\theta_p^\epsilon = \arcsin \left(\frac{n_a}{n_p^\epsilon} \sin \theta_p \right). \quad (11)$$

For simplicity, $\theta_b' \equiv \theta_b^H$ in the reminder of the paper.

In the present work, the birefringent crystal is tilted around the laboratory vertical axis, which is parallel to the vertical polarization and perpendicular to the optical table, as shown in Fig. 3. Furthermore, the optic axis \vec{c} of the crystal lies on the horizontal plane, which means that the angle θ_c' between \vec{c} and the beam propagation direction changes as the crystal is allowed to rotate around the vertical axis. In this arrangement, the refractive index is constant for the vertical (ordinary) polarization, whereas the effective refractive index for the horizontal (extraordinary) polarization changes as the crystal is tilted according to⁷,

$$n_b^H = \left[\frac{\cos^2(\theta_c')}{n_o^2} + \frac{\sin^2(\theta_c')}{n_e^2} \right]^{-\frac{1}{2}}, \quad (12)$$

with n_o and n_e the ordinary and extraordinary refractive indices of the birefringent crystal, respectively, and θ_c' defined as $\theta_c' = \theta_c + \theta_b'$. We allow for the fact that the chosen crystal might potentially be cut so that crystal

axis \vec{c} is at an angle θ_c to the crystal face normal. For the vertical polarization, n_b^V is identically equal to n_o , whereas for the horizontal polarization the refractive index n_b^H depends on the crystal tilt, as seen from the last equation.

According to Eq. (12), one must know θ_b' to find n_b^H , but at the same time one needs n_b^H to get θ_b' by means of Eq. (11). Unfortunately, this pair of equations do not have analytic solution for θ_b' and n_b^H . So, in order to be able to contrast the experimental results in Sec. IV with the theoretical predictions, n_b^H is estimated in the following way. First, θ_b' is approximated by θ_b in Eq. (12), resulting in $\theta_c' \approx \theta_c + \theta_b$ which is used to find a zero-order approximation for n_b^H . Second, using this result, a value for θ_b' is calculated via Eq. (11). Third, that result for θ_b' is substituted in Eq. (12) to finally obtain a first-order approximation for n_b^H . Repeating the same steps, a second-order approximation for n_b^H can be calculated. The discrepancy between the zero- and first-order approximations is less than 0.5% and between the first- and second-order approximations is less than 0.004%. In this paper, the second-order approximation is used.

III. EXPERIMENTAL REALIZATION

The Mach-Zehnder interferometer shown in Fig. 2 can be used to implement a VPPBS. However, depending on its spatial dimensions and external factors like vibrations and air currents, this interferometer might require active phase stabilization in order to hold a specific set of T and R coefficients for a long period of time, e.g. hours. A variation of the Mach-Zehnder interferometer, called a displaced Sagnac interferometer^{8–10}, is used instead to reduce this inherent instability. In this, the light is split by and returns to the same NPBS using three mirrors, as shown in Fig. 3. The two counter-propagating beams inside the interferometer play the same role as the two arms in a Mach-Zehnder. In the non-displaced version of the Sagnac interferometer, the counter-propagating beams inside the interferometer follow exactly the same paths. This makes it difficult to introduce a relative phase between the beams, as it is required in the current scheme. It also means that beam in Output 1 exits along the exact path of the input beam, which makes the output beam difficult to access. A displaced Sagnac eliminates these issues. In it, one translates the mirror in the Sagnac that is diagonally opposite to the NPBS. This separates the two counter-propagating paths, while maintaining their collinearity.

Given that the transverse separation between the paths is small (~ 2 cm) compared to the footprint of the interferometer ($70 \text{ cm} \times 70 \text{ cm}$), and the fact that the beams are reflected and transmitted by the same mirrors and NPBS in the interferometer, any vibration or air current affects both optical paths roughly in the same way, making the Sagnac interferometer stable without active

TABLE I. Comparison between tilted optical medium and liquid crystal methods to control the relative phase in the displaced Sagnac interferometer in Fig. 3.

	Tilted birefringent crystal and glass plate	Liquid crystals
Advantages	Need to align axis only for the birefringent crystal	ϕ_H and ϕ_V each have their own control
	Induced phase is stable over months	Normal incidence (i.e. no beam displacement), implying bigger aperture for a given device width
	Tilted medium is usable to its edge, which allows for counterpropagating beam clearance	
Disadvantages	ϕ_H and ϕ_V are not independently controlled	Need to align axes for both liquid crystals
	Refractive beam displacement can reduce interference visibility	Liquid crystal response can change from one voltage ramp to the next
	Requires a precision rotation mount (e.g. vernier)	Since they are not usable up to their edge, a large Sagnac path separation is required
		Easy to damage with a DC voltage

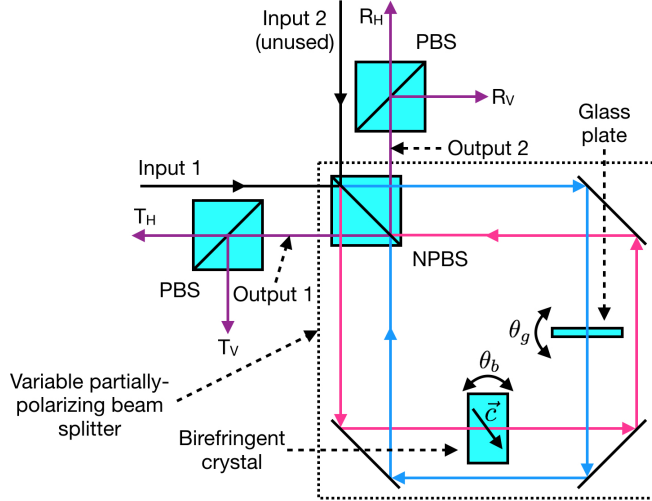


FIG. 3. Experimental realization of a variable partially-polarizing beam splitter using a displaced Sagnac interferometer composed of three mirrors and a non-polarizing beam splitter (NPBS). Two polarizing beam splitters (PBSs) have been placed at each output port to study the transmission and reflection coefficients for each polarization. The thickness of the birefringent crystal has been exaggerated to indicate the orientation of its optic axis \vec{c} .

stabilization⁹.

IV. EXPERIMENTAL RESULTS

To demonstrate the working principle of a VPPBS based on the Sagnac interferometer in Fig 3, the four

The experiment was carried out using a HeNe laser in free space with wavelength $\lambda = 632.8$ nm. The displaced Sagnac interferometer was built using a broadband (400 - 700 nm) 50:50 NPBS cube with 2.54 cm side length (Thorlabs BS013) and three 5.08 cm diameter silver mirrors. As mentioned above, the phase retarders can be either two liquid crystals driven by an AC voltage or a birefringent crystal plus a glass plate tilted as shown in Fig. 3. However, only the second case was investigated here since such elements are easily accessible in the laboratory. For a full comparison between the tilted optical medium and liquid crystal methods we refer the reader to the Table I. The birefringent crystal was a β barium borate (BBO) crystal of nominal thickness $d_b = 0.245$ mm and nominal optic axis at $\theta_c = 33.4^\circ$; the glass plate was a microscope cover slide of nominal thickness $d_g = 0.16$ mm. These two elements were mounted in automated rotation stages and tilted between -10° and 10° in steps of 0.1° for θ_b and 0.25° for θ_g . The input light was diagonally polarized by means of a polarizing beam splitter (PBS) plus a half-wave plate with its fast axis at 22.5° with respect to the horizontal direction. As seen in Fig. 3, at each output port of the VPPBS a PBS was placed to study the T and R coefficient for both polarizations. The intensities were recorded for each value of θ_b and θ_g by four photodiodes after averaging 100 measurements taken over 2 seconds.

coefficients T_H , T_V , R_H and R_V were measured as described in Sec. III and are shown in Fig. 4(a).

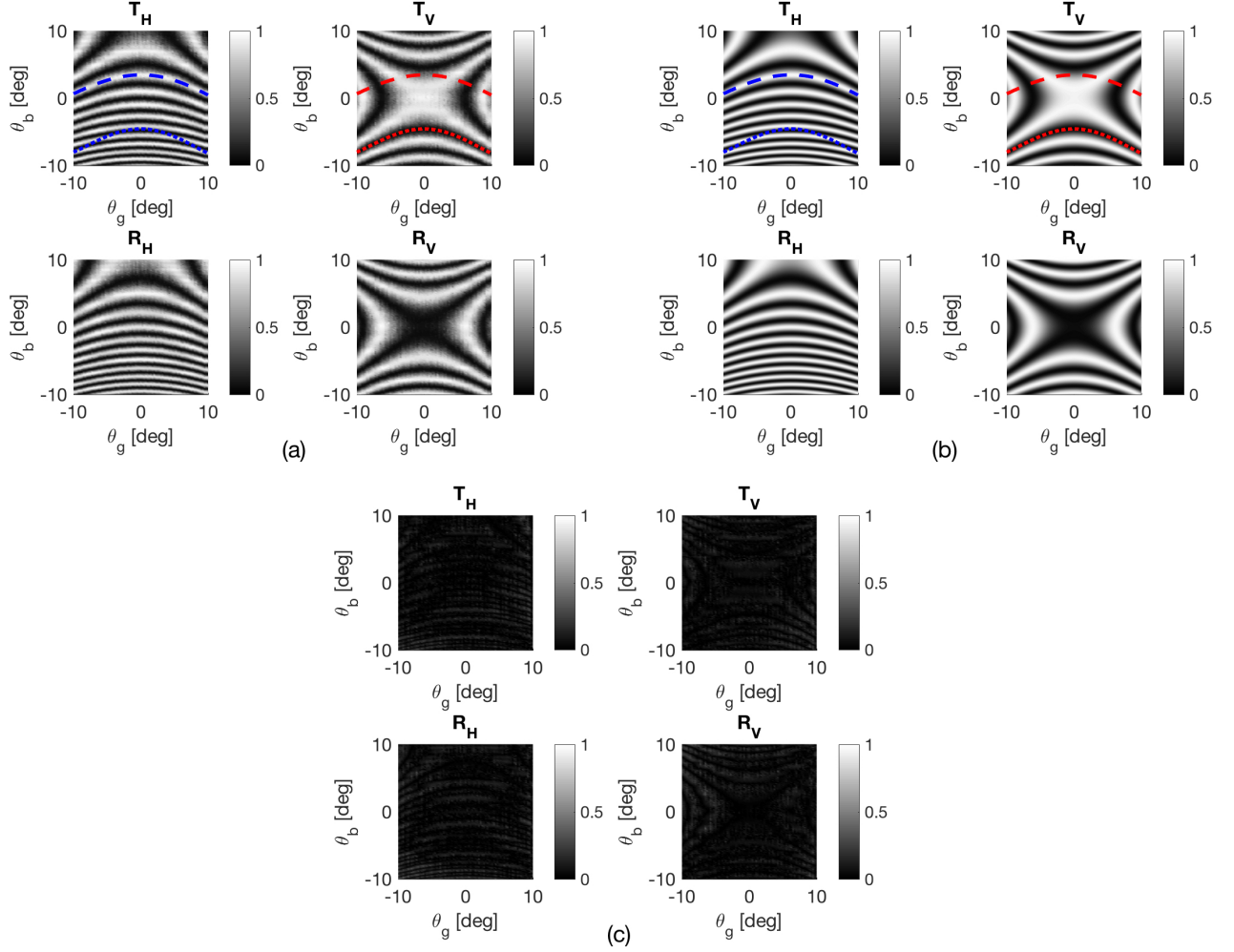


FIG. 4. (a) Experimental transmission T and reflection R coefficients for the horizontal H and vertical V polarizations in the output ports of the variable partially-polarizing beam splitter shown in Fig. 3. The axes, θ_b and θ_g , are the tilts of the birefringent crystal and glass plate, respectively. (b) Theoretically expected T and R coefficients for the H and V polarizations of the variable partially-polarizing beam splitter in Fig. 3 according to the theoretical model in Sec. II and the fitting procedure explained in Sec. IV. (c) Absolute difference between experiment and theory. The maximum absolute difference for each coefficient is 0.36 (T_H), 0.39 (T_V), 0.43 (R_H), and 0.41 (R_V). The dashed and dotted lines in (a) and (b) correspond to the bands used to illustrate a complete and independent control of the variable partially-polarizing beam splitter coefficients in Fig. 5.

The first observation in Fig. 4(a) is that the VPPBS coefficients exhibit several maxima and minima in the range of θ_b and θ_g values studied here. At these points there is either constructive or destructive interference due to the relative phases introduced by the birefringent crystal and glass plate. As expected, the T_H and R_H coefficients are complementary to one another, i.e. when T_H is maximum R_H is minimum and vice versa. This complementarity happens as well for T_V and R_V . Furthermore, the coefficients in Fig. 4(a) are symmetric with respect to the axis $\theta_g = 0$, which comes from the fact that the relative phase introduced by the glass plate is the same for both positive and negative θ_g angles. The same happens for T_V and R_V with respect to the axis $\theta_b = 0$ since n_b^V is a constant. In contrast, T_H and R_H are asym-

metric with respect to the axis $\theta_b = 0$ because the angle θ_c of the optic axis \vec{c} is not zero when the face of the birefringent crystal is perpendicular to the beam. This creates a difference between a positive or negative tilt of the crystal that only affects the horizontal polarization, in accordance with Eq. (12).

In order to compare the experimental results in Fig. 4(a) with the theoretical model in Sec. II, Eqs. (7)-(12), a least-squares fitting of the experimental data is performed in the following way. First, the experimental visibilities for the four coefficients in Fig. 4(a) are taken into account in the theoretical model by using a modified version of Eq. (7),

$$T_\epsilon = \frac{1 + \mathcal{V}_\epsilon \cos \phi_\epsilon}{2}, \quad (13)$$

where \mathcal{V}_ϵ is the experimental visibility for the coefficient T_ϵ ($\epsilon = H, V$). The reflection coefficients are still given by $R_\epsilon = 1 - T_\epsilon$. Second, the thicknesses d_b and d_g for the phase retarders are adjusted iteratively using only T_V in Fig. 4(a) since the index of refraction for the V polarization is a constant and therefore independent of θ_c , the third fitted parameter described below (R_V could have been used as well). The adjusted values for d_b and d_g are 0.2724 mm and 0.1477 mm, respectively. Third, using these adjusted thicknesses, the experimental coefficient T_H is iteratively fitted using θ_c and a tilt angle offset θ_0 for the birefringent crystal (such that $\theta_b \rightarrow \theta_b + \theta_0$) as fitting parameters. The results for θ_c and θ_0 are respectively 32.14° and 0.061° . Finally, the four adjusted parameters are introduced in the theoretical model and the resulting coefficients are depicted in Fig. 4(b). The values for the refractive indices are $n_g = 1.5151$ (BK7 refractive index¹¹), and $n_o = 1.6672$ and $n_e = 1.5496$ (from the Sellmeier's equations¹² for BBO at $\lambda = 632.8$ nm).

In order to easily compare the experimental results to the theory in Fig. 4, a plot showing the absolute difference between the two is presented in Fig. 4(c). Qualitatively, the theoretical model reproduces the experimental VPPBS performance. However, even after all the careful fitting described above, the maximum absolute difference, 0.43, is remarkably large. The refractive indices are the only parameters that were not fitted, which suggests that they may be a contributor to this discrepancy. In any case, we conclude that the theoretical model is insufficiently accurate to predict the required tilt angles for a desired transmission coefficient. Instead, the experimental characterization in Fig. 4(a) must be used.

The VPPBS working principle can be illustrated using Fig. 4(a) by finding the tilt angles at which one of the transmission coefficients is kept constant while the other varies. As example, it is shown here the case when T_H is kept constant while T_V varies. This can be accomplished by selecting any band in the T_H plot for which this coefficient is constant, e.g. the one marked with a dashed (blue) line in Fig. 4(a). For the same tilt angles that describe such a line in the T_H contour plot, a set of values between 0 and 1 is found for the T_V coefficient, as indicated by a dashed (red) line in Fig. 4(a). The latter case is illustrated in Fig. 5(a), where the T_H and T_V coefficients are shown as a function of θ_g that parametrizes the dashed line in Fig. 4(a). In Fig. 5(b) a second case is considered, T_V set to its minimum value while T_H is varied. One of the bands in the plot for T_V in Fig. 4(a) that fulfills this condition is highlighted with a dotted (red) line. In this case, the T_H coefficient achieves values between 0 and 1 indicated by a dotted (blue) line in Fig. 4(a). Therefore, by selecting an appropriate value for θ_g that parametrizes the dotted line, it is possible to get an arbitrary value for T_H .

The two cases summarized in Fig. 5 illustrate the fact that the T_H and T_V coefficients, and therefore their reflection counterparts, can be controlled at will by choos-

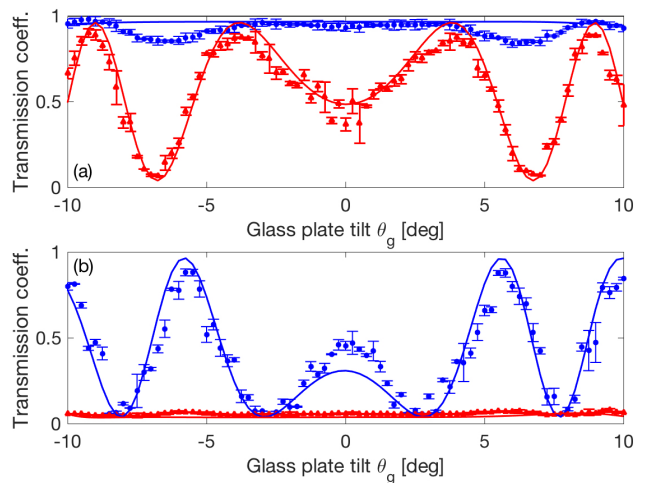


FIG. 5. Transmission coefficients for the horizontal (blue circles) and vertical (red triangles) polarizations in two particular cases: (a) when T_H is maximum and T_V varies, and (b) when T_V is minimum and T_H varies. These two plots respectively correspond to the dashed and dotted lines in Fig. 4(a). The solid curves correspond to the theoretical transmission coefficients along the same two lines. In order to be visible, the error bars correspond to three times the standard deviation over the 100 measurements taken for each data point. The noise observed is mainly due to laser instability arising from back reflections.

ing two tilt angles. In other words, the relative phases introduced by the birefringent crystal and glass plate allow a complete and independent control of the T and R coefficients for both polarizations, which is the defining feature of a VPPBS.

The performance of the VPPBS presented here can be quantified in terms of the interferometer visibility for each polarization. On one hand, the overall visibility for the H polarization (T_H coefficient in Fig. 4(a)) was 93%, while for the V polarization (T_V coefficient in Fig. 4(a)) was 92%. In the particular cases shown in Fig. 5, the T_V (panel (a)) and T_H (panel (b)) coefficients display visibilities of 89% and 86%, respectively. We have considered and ruled out a number of possible sources for the imperfect visibility, including imbalanced NPBS splitting ratios, fluctuations in the signal, and polarization. This leaves the most likely source to be alignment of the interferometer. In any case, the main impact of imperfect visibility will be to limit the achievable range of the transmission coefficient, as can be seen in Eq. (13). Despite this fact, the Sagnac interferometer remained stable over 12 hours without the need for active feedback or constant readjustment, which suggests that the VPPBS could successfully be used as an element in a larger experimental setup.

Lastly, we discuss the theoretical lines in Fig. 5. Qualitatively, the strongly varying transmission coefficients in panels (a) (red curve) and (b) (blue curve) follow the behaviour of the experimental points. However, the trans-

mission coefficients that are meant to be constant do vary unlike their corresponding theoretical curves. Moreover, for all four curves, the discrepancy between theory and experiment is greater than the experimental uncertainty for most data points. Given the low accuracy of the theoretical model and its relative complexity, this discrepancy again confirms that it is better to use the experimental characterization of the VPPBS presented in Fig. 4(a) to determine the correct tilt media angles for a target transmission coefficient.

V. CONCLUSIONS

A variable partially-polarizing beam splitter is presented based on a displaced Sagnac interferometer. The transmission and reflection coefficients for the horizontal and vertical polarizations are controlled via the tilts of a birefringent crystal and a glass plate, which introduce a relative phase to each polarization. The overall effect of these two phase retarders is a complete and independent manipulation of the VPPBS splitting ratios for the two polarizations. Since this design includes optical elements that can be found in any optics laboratory, its implementation is straightforward and inexpensive.

This work was supported by the Canada Research Chairs (CRC) Program, the Natural Sciences and Engineering Research Council (NSERC), and the Canada Excellence Research Chairs (CERC) Program. JF acknowledges support from COLCIENCIAS.

- ¹N. Kiesel, C. Schmid, U. Weber, R. Ursin, and H. Weinfurter, “Linear optics controlled-phase gate made simple,” *Phys. Rev. Lett.* **95**, 210505 (2005).
- ²R. Okamoto, H. F. Hofmann, S. Takeuchi, and K. Sasaki, “Demonstration of an optical quantum controlled-not gate without path interference,” *Phys. Rev. Lett.* **95**, 210506 (2005).
- ³N. K. Langford, T. J. Weinhold, R. Prevedel, K. J. Resch, A. Gilchrist, J. L. O’Brien, G. J. Pryde, and A. G. White, “Demonstration of a simple entangling optical gate and its use in Bell-state analysis,” *Phys. Rev. Lett.* **95**, 210504 (2005).
- ⁴A. Ling, K. P. Soh, A. Lamas-Linares, and C. Kurtsiefer, “Experimental polarization state tomography using optimal polarimeters,” *Phys. Rev. A* **74**, 022309 (2006).
- ⁵Z. E. D. Medendorp, F. A. Torres-Ruiz, L. K. Shalm, G. N. M. Tabia, C. A. Fuchs, and A. M. Steinberg, “Experimental characterization of qutrits using symmetric informationally complete positive operator-valued measurements,” *Phys. Rev. A* **83**, 051801 (2011).
- ⁶F. Kaiser, T. Coudreau, P. Milman, D. B. Ostrowsky, and S. Tanzilli, “Entanglement-enabled delayed-choice experiment,” *Science* **338**, 637 (2012).
- ⁷R. W. Boyd, *Nonlinear Optics, Third Edition*, 3rd ed. (Academic Press, 2008).
- ⁸T. Nagata, R. Okamoto, J. L. O’Brien, K. Sasaki, and S. Takeuchi, “Beating the standard quantum limit with four-entangled photons,” *Science* **316**, 726 (2007).
- ⁹M. Mičuda, E. Doláková, I. Straka, M. Miková, M. Dušek, J. Fiurásek, and M. Ježek, “Highly stable polarization independent Mach-Zehnder interferometer,” *Review of Scientific Instruments* **85**, 083103 (2014).
- ¹⁰J. M. Ashby, P. D. Schwarz, and M. Schlosshauer, “Observation of the quantum paradox of separation of a single photon from one of its properties,” *Physical Review A* **94**, 012102 (2016).

- ¹¹Schott, “Optical glass data sheets,” (2015).
- ¹²K. Kato, “Second-harmonic generation to 2048 Å in beta-BaB₂O₄,” *IEEE Journal of Quantum Electronics* **QE-22**, 1013 (1986).
- ¹³Y.-C. Jeong, J.-C. Lee, and Y.-H. Kim, “Experimental implementation of a fully controllable depolarizing quantum operation,” *Physical Review A* **87**, 014301 (2013).
- ¹⁴A. Cuevas, M. Proietti, M. A. Ciampini, S. Duranti, P. Mataloni, M. F. Sacchi, and C. Macchiavello, “Experimental detection of quantum channel capacities,” *Physical Review Letters* **119**, 100502 (2017).
- ¹⁵J. L. O’Brien, G. J. Pryde, A. G. White, T. C. Ralph, and D. Branning, “Demonstration of an all-optical quantum controlled-not gate,” *Nature* **426**, 264 (2003).
- ¹⁶P. G. Evans, R. S. Bennink, W. P. Grice, T. S. Humble, and J. Schaake, “Bright source of spectrally uncorrelated polarization-entangled photons with nearly single-mode emission,” *Phys. Rev. Lett.* **105**, 253601 (2010).

Appendix A: Alternative VPPBS configurations

A VPPBS can also be created using a variation of the Mach-Zehnder interferometer in Fig. 2. As shown in Fig. 6, by replacing the NPBSs by PBSs and implementing the phase retarders via half-wave plates (HWPs), similar expressions for $\mathbf{E}_{\text{out},1}(t)$ and $\mathbf{E}_{\text{out},2}(t)$ in Eqs. (5) and (6) are obtained. Indeed, the interferometer in Fig. 6 has its own displaced Sagnac-interferometer version presented in Refs.^{13,14}, except for the HWP at 45° in one of its outputs. The main reason to implement experimentally the Sagnac interferometer in Fig. 3 instead of the one in Refs.^{13,14} is that the separation between the counter-propagating paths does not provide enough room to place the HWP rotating mounts at our disposal without blocking one of the beams.

To see explicitly how the Mach-Zehnder interferometer in Fig. 6 works as a VPPBS, consider light entering at Input 1 with the electric field $\mathbf{E}_{\text{in}}(t)$ in Eq. 1. After the first PBS the upper and lower fields read

$$\mathbf{E}_{\text{upper}}(t) = \begin{bmatrix} E_{\text{in}}^H(t) \\ 0 \end{bmatrix}, \quad (\text{A1})$$

$$\mathbf{E}_{\text{lower}}(t) = e^{i\frac{\pi}{2}} \begin{bmatrix} 0 \\ E_{\text{in}}^V(t) \end{bmatrix}. \quad (\text{A2})$$

After the HWPs with fast axes oriented at θ_H and θ_V in the upper and lower paths, respectively, the electric fields become

$$\tilde{\mathbf{E}}_{\text{upper}}(t) = E_{\text{in}}^H(t) \begin{bmatrix} \cos(2\theta_H) \\ \sin(2\theta_H) \end{bmatrix}, \quad (\text{A3})$$

$$\tilde{\mathbf{E}}_{\text{lower}}(t) = e^{i\frac{\pi}{2}} E_{\text{in}}^V(t) \begin{bmatrix} \sin(2\theta_V) \\ -\cos(2\theta_V) \end{bmatrix}. \quad (\text{A4})$$

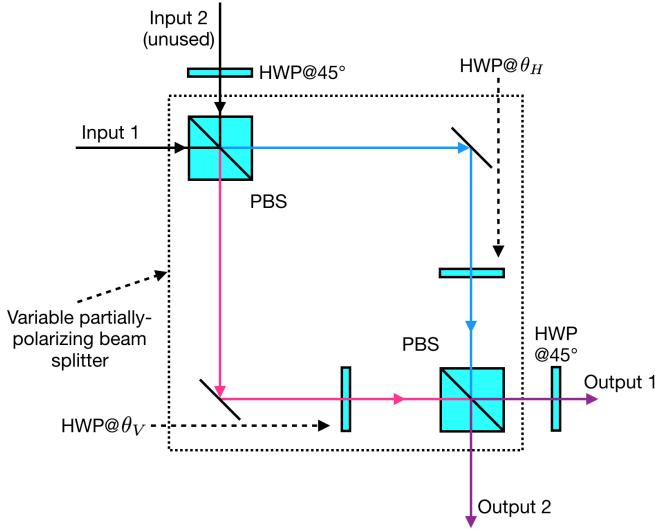


FIG. 6. Variable partially-polarizing beam splitter based on a Mach-Zehnder interferometer with polarizing beam splitters (PBSs) instead of non-polarizing beam splitters as in Fig. 2, and half-wave plates (HWPs) as phase retarders. Although Input 2 is unused in the current description of the VPPBS, a HWP at 45° must be placed at this input to convert the horizontal polarization at Input 2 to vertical so that it travels into the same arm as the horizontal polarization at Input 1. Consequently, the two inputs can then be mixed by the HWP in that arm. A similar argument holds for the vertical polarizations at Input 1 and 2. This HWP at Input 2 is necessary when both inputs of the VPPBS are required, as in two-photon quantum logic gate operations^{1-3,15}.

Finally, at Outputs 1 and 2, including the HWP at 45° in the first one, the electric fields are

$$\mathbf{E}_{\text{out},1}(t) = \begin{bmatrix} E_{\text{in}}^H(t) \sin(2\theta_H) \\ E_{\text{in}}^V(t) \sin(2\theta_V) \end{bmatrix}, \quad (\text{A5})$$

$$\mathbf{E}_{\text{out},2}(t) = \begin{bmatrix} E_{\text{in}}^H(t) \cos(2\theta_H) \\ E_{\text{in}}^V(t) \cos(2\theta_V) \end{bmatrix}. \quad (\text{A6})$$

These expressions are physically identical to Eqs. (5) and (6), and therefore allow the definition of the VPPBS transmission and reflection coefficients as in Eq. (7).

Alternatively, PBSs in Fig. 6 can be implemented using two birefringent walk-off crystals (e.g. calcite) in a linear configuration^{15,16}. The VPPBS based on the resulting interferometer is shown in Fig. 7. In this design, the separation between optical paths is small and all paths pass through the same crystals. Consequently, much like the displaced Sagnac interferometer, this linear interferometer exhibits an inherent phase stability.

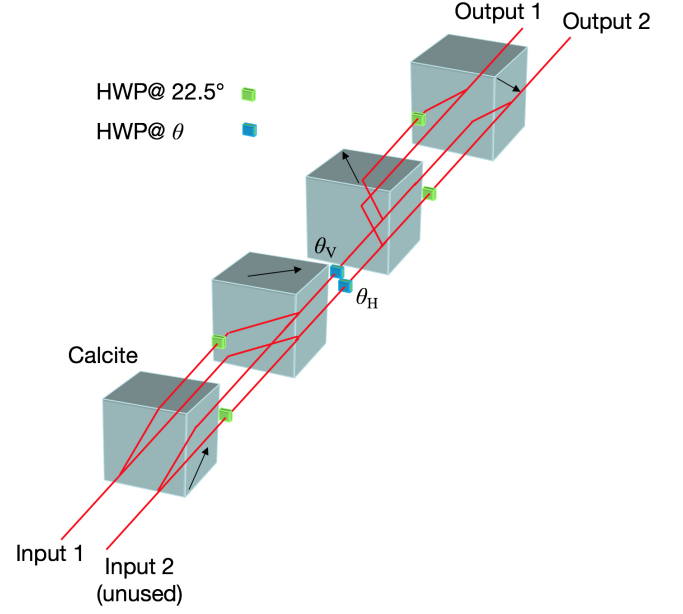


FIG. 7. Alternative VPPBS configuration using PBSs made of birefringent crystals in a linear configuration. The resulting interferometer exhibits phase stability, much like the displaced Sagnac interferometer described in the main part of the paper. The arrow on each walk-off crystal indicates the direction of its optic axis.

Appendix B: Phase introduced by a tilted optical plate

In Sec. II, the relative phase ϕ in Eq. (10) is obtained as follows. Consider an optical medium of thickness d and refractive index n that is tilted by an angle θ , as shown in Fig. 8. As mentioned in Sec. II, when the optical medium is perpendicular to the input beam the relative phase between the optical paths in a Mach-Zehnder interferometer is given by

$$\phi = \frac{2\pi d}{\lambda} (n - n_a), \quad (\text{B1})$$

with λ the light wavelength and n_a the refractive index of air. When the optical medium is tilted, the relative phase between the two optical paths corresponds to

$$\phi = \frac{2\pi \ell}{\lambda} n - \frac{2\pi(d + \delta)}{\lambda} n_a, \quad (\text{B2})$$

where ℓ is the length that light travels through the optical medium, and δ is a small length that, together with d , defines the longitudinal component of ℓ . One can understand Eq. (B2) considering two optical media, the first one of thickness ℓ and refractive index n in one arm of the interferometer and the second one of thickness $d + \delta$ and refractive index n_a (“made” of air) in the other arm.

According to Fig. 8, ℓ is equal to

$$\ell = \frac{d}{\cos \theta}, \quad (\text{B3})$$

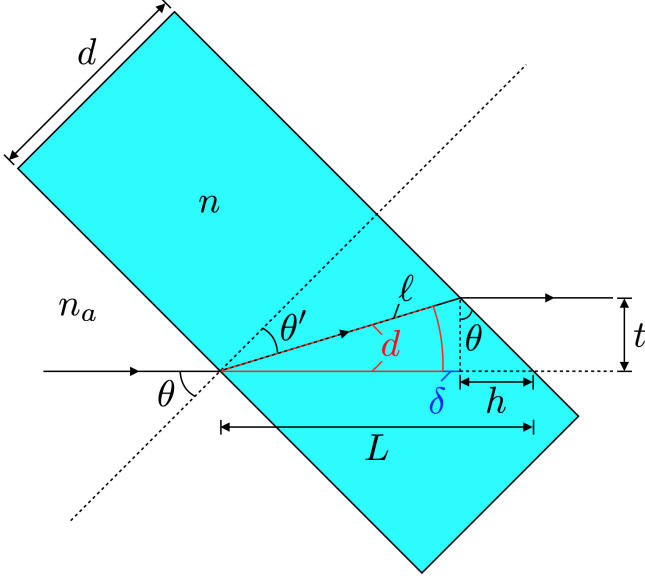


FIG. 8. Optical medium of thickness d and refractive index n tilted by an angle θ . Such an angle has been exaggerated to introduce all the important quantities in the calculation of the relative phase ϕ in Eq. (10).

where θ' is the angle of refraction given by Snell's law in Eq. (11). In terms of ℓ , the transverse separation t between the input and output beams is equal to

$$t = \ell \sin(\theta - \theta') = \frac{d}{\cos \theta'} \sin(\theta - \theta'), \quad (\text{B4})$$

allowing to find an expression for h in Fig. 8,

$$h = t \tan \theta = \frac{d}{\cos \theta'} \sin(\theta - \theta') \tan \theta. \quad (\text{B5})$$

On the other hand, the quantity L , defined as the total length that light would travel through if there were no optical medium, is

$$L = \frac{d}{\cos \theta}. \quad (\text{B6})$$

However, according to Fig. 8, $d + \delta$ is equal to $L - h$. Thus the relative phase in Eq. (B2) becomes

$$\phi = \frac{2\pi\ell}{\lambda} n - \frac{2\pi(L - h)}{\lambda} n_a. \quad (\text{B7})$$

Substituting Eqs. (B3), (B5) and (B6) into the last expression, ϕ reduces to

$$\phi = \frac{2\pi d}{\lambda} \times \left[\frac{n}{\cos \theta'} - n_a \left(\frac{1}{\cos \theta} - \frac{\sin(\theta - \theta') \tan \theta}{\cos \theta'} \right) \right], \quad (\text{B8})$$

which can be simplified to finally obtain Eq. (10) in Sec. II,

$$\phi = \frac{2\pi d}{\lambda} \left[\frac{n}{\cos \theta'} - n_a (\cos \theta + \sin \theta \tan \theta') \right]. \quad (\text{B9})$$